IEEE Access
Multidisciplinary ⋮ Rapid Review ⋮ Open Access Journal

Received 15 August 2022, accepted 1 September 2022, date of publication 5 September 2022, date of current version 15 September 2022.

Digital Object Identifier 10.1109/ACCESS.2022.3204270

RESEARCH ARTICLE

Fuzzy State-Dependent Riccati Equation (FSDRE) Control of the Reverse Osmosis Desalination System With Photovoltaic Power Supply

HOSSEIN DARVISHI NEJAD[1], MOSTAFA NAZARI[1], MOHSEN NAZARI[1], MOHAMMAD MOHSEN SHAH MARDAN[1], ARDASHIR MOHAMMADZADEH[2], (Student Member, IEEE), MAI THE VU[3], AND AMIR MOSAVI[4,5,6], (Student Member, IEEE)

[1]Faculty of Mechanical and Mechatronics Engineering, Shahrood University of Technology, Shahrud, Iran
[2]Multidisciplinary Center for Infrastructure Engineering, Shenyang University of Technology, Shenyang 110870, China
[3]School of Intelligent Mechatronics Engineering, Sejong University, Seoul 05006, South Korea
[4]John von Neumann Faculty of Informatics, Obuda University, 1034 Budapest, Hungary
[5]Institute of Information Engineering, Automation and Mathematics, Slovak University of Technology in Bratislava, 811 07 Bratislava, Slovakia
[6]Institute of Information Society, University of Public Service, 1083 Budapest, Hungary

Corresponding authors: Mostafa Nazari (amir.mosavi@kvk.uni-obuda.hu), Mai The Vu (maithevu90@sejong.ac.kr), and Amir Mosavi (amir.mosavi@mailbox.tu-dresden.de)

ABSTRACT The two challenges facing human life are water and energy. Reverse osmosis (RO) desalination systems are popular owning to their unique advantages. However, robust performance and power supply are the two main challenges in this desalination system. This power is used to drive an induction motor that rotates a centrifugal pump to apply the required back pressure to the RO membrane. To solve these two challenges, a complete RO system powered by a photovoltaic (PV) system was considered, and for each subsystem, a robust controller was designed based on their dynamic models. A fuzzy controller optimized by the invasive weed algorithm (IWA) was designed to track the maximum power in the photovoltaic subsystem under different environmental conditions. A fuzzy-PID controller was used to control the motor-pump subsystem. Furthermore, it is focused on designing a robust controller with the ability to compensate for large set-point changes, reject external disturbances, and cope with parametric uncertainties, such as variations in feed water salinity. Hence, state-dependent Riccati equation control (SDRE) was used to control the reverse osmosis system. The simulation results for different scenarios show that the proposed controller performs well under different operating conditions and can remove the effects of disturbances on the system.

INDEX TERMS Fuzzy control, maximum power point tracking, photovoltaic system, reverse osmosis desalination, SDRE control, artificial intelligence.

I. INTRODUCTION

Water and energy are the two main needs of human life. Only 1% of water in the world is suitable for drinking or industrial purposes [1]. There are various methods for the desalination of salt water, and each of them has its advantages and disadvantages [2]. Based on the UNESCO report, by 2030, up to 40% of the world people will be influenced by water shortage [3]. Since about 97% of water in the world is saline water, the main solutions to achieve freshwater are desalination and reusing the water [4], [5]. The desalination process, which refers to the process of separating a special part of a water-soluble salt, is categorized as membrane-based methods and evaporation-based methods [2]. In both of them, the incoming saline water is divided into freshwater and water with higher salinity (Brine water). But, in some cases, pre-treatment units are required before the water enters the desalination unit, and then a post-treatment unit is required [6]. The reverse osmosis desalination system, despite its high maintenance cost, has advantages; its design and operation is simple and has low

The associate editor coordinating the review of this manuscript and approving it for publication was Ton Duc Do.

energy usage [7]. Also, with the development of membranes that need lower pressure behind them, the use of such systems in desalination will become more pervasive [8].

In desalination systems, consumption of energy is a crucial factor, and even the presence of this barrier has sometimes prevented the use of such systems. Reverse osmosis (RO) systems require electricity to run their electric motors. Therefore, in places that do not have access to electricity, it is practically impossible to use such systems. In many parts of the world, people will be forced to move to another place due to the lack of electricity. Also, due to the lack of freshwater, agriculture will practically disappear in such areas. Using renewable energy such as solar energy can overcome this issue which is available in many places [9], [10], [11], [12]. Solar energy accounts for up to 57% of the market of the renewable energy-based desalination, which the main is RO desalination system supplied by photovoltaic (PV) energy [11], [13]. A technical-economic feasibility study has been done for a PV-RO system in [14]. In [15],a state of the art in wind and solar energy-driven RO is presented. Therefore, in this paper, the energy supply of the RO system is regarded as the photovoltaic system [11], [12].

However, this system has some limitations similar to other systems. Some limitations are related to the system. For example, the performance of the PV system is related to some parameters such as the temperature and the sunlight intensity, which differ from one place to another; the maintenance of the RO system is costly, and pre and post-treatment may be essential.

There are some researches on controlling the reverse osmosis system process which many have regarded the linear model of the RO system. For example, In [16] and [17], the authors have considered an industrial RO system using traditional PID controller. The controller for stabilizing the linear reverse osmosis system around the desired point was proposed in [18]. However, some papers have considered the control of the nonlinear model of the reverse osmosis system. In [19], a nonlinear feedback/feedforward control is provided. In [20], a controller based on a nonlinear model has been designed and implemented on the reverse osmosis desalination laboratory system which used geometric control methods. The influence of the variable frequency drive (VFD) and the pressure regulating valve on the reverse osmosis desalination system were experimentally studied in [21]. The combined photovoltaic-reverse osmosis (PV-RO) system was studied in [22], but only the maximum power point tracking of the photovoltaic system was considered. The Model Reference Adaptive Control (MRAC) method was used for controlling the combined PV-RO system in [23]. In [24], the model predictive control approach was used for fault-tolerant control of a small reverse osmosis system.

The disadvantage of these researches is that they do not include the necessary elements for the reverse osmosis system such as power supply, pumping process, and some others like them. From our knowledge, only [25], [26] has considered these elements. In [25], the super-twisting approach has been considered in controlling the RO desalination system besides other elements.

A slap optimization-based PID controller has been designed in [27] for a PV-RO system. However, the linear model of the system has been considered and there are no details of other elements in the system.

A new control strategy for minimization of energy was proposed in [28] by manipulating feed pressure and reject valve opening. In [29], energy management and control of renewable energy-powered reverse osmosis desalination systems without batteries are proposed.

According to the above points, in this paper, the complete set of the photovoltaic solar system, pump and electric motor system, and reverse osmosis system membrane are examined together. Maximum power point tracking (MPPT) in different environmental (temperature and radiation) conditions of the PV solar system, an optimized fuzzy controller with an invasive weed algorithm (IWA) is used, which is much more efficient than classical algorithms such as hill-climbing [30]. A fuzzy-PID controller is considered to control the motor-pump subsystem. This controller is more robust than the classical PID controller and performs better in nonlinear systems. Moreover, a novel application of state-dependent Riccati equation (SDRE) control is also proposed to regulate the flow rates in the reverse osmosis system in integration with the motor-pump subsystem and photovoltaic subsystem.

Therefore, the main contributions of this paper are as follows:

- Considering the PV-powered reverse osmosis (RO) desalination system in integration with other essential elements
- Using the SDRE method for control of the reverse osmosis subsystem
- Using Fuzzy-IWA controller for MPPT of photovoltaic subsystem
- Evaluating the closed-loop system in dealing with different uncertainties and disturbances

The aim of the proposed control design is to reach proper dynamic performance and compensate for the effects of noise and uncertain parameters.

The structure of the paper is as follows. In the next section, the combined RO system powered by photovoltaic system is presented. The controller design for each part is presented in section 3. The simulation results are in section 4, and then the conclusions are in the final section.

II. THE COMBINED REVERSE OSMOSIS-PHOTOVOLTAIC SOLAR (PV-RO) SYSTEM

Fig. 1 shows the structure of the closed-loop system. As shown in this figure, the system has the following components:

- A photovoltaic solar generator with an energy management block
- DC-DC boost converter, which the MPPT is done by adjusting its duty cycle in different radiation and temperature conditions.

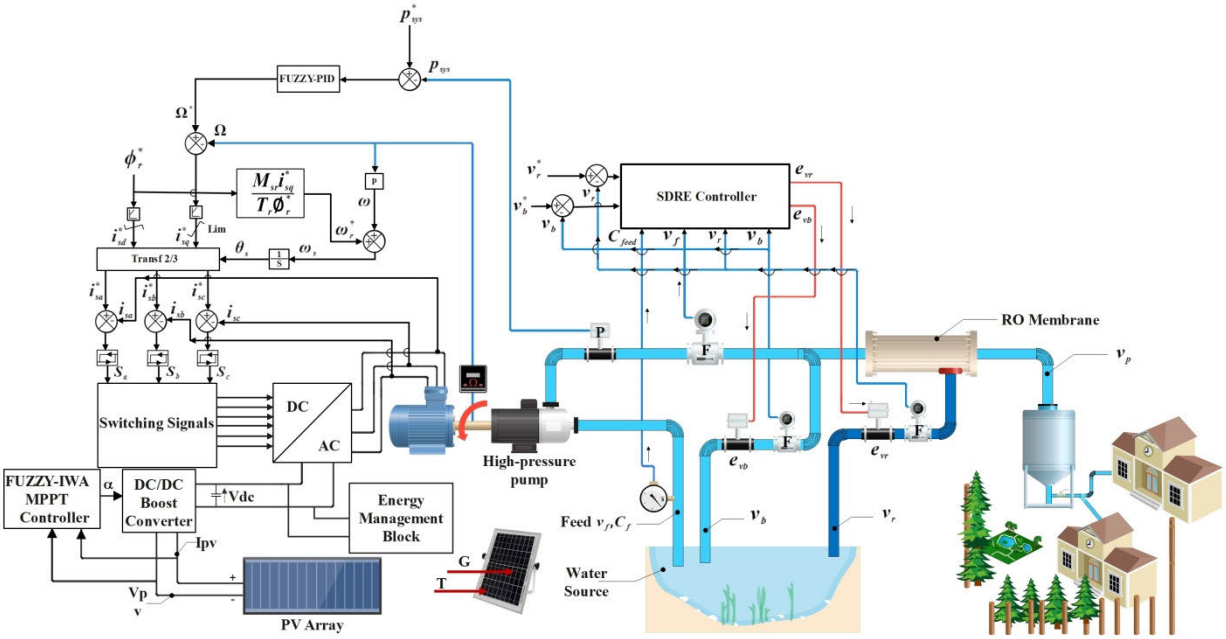

FIGURE 1. Combination of the reverse osmosis desalination system and the photovoltaic system.

- DC-AC three-phase inverter
- Induction motor-centrifugal pump subsystem
- Reverse osmosis membrane

In this configuration, a system that can produce freshwater from various water sources using sustainable energy is considered.

In the following, we will describe each of the components in more detail.

A. PHOTOVOLTAIC SOLAR SUBSYSTEM

The solar system is used to generate electricity to power the induction motor connected to the centrifugal pump. Several mathematical models have been proposed to describe the performance of a photovoltaic generator [31], [32], [33]. Fig. 2 shows the single diode circuit of a solar cell.

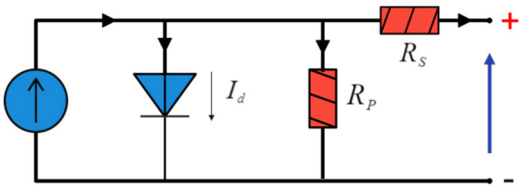

FIGURE 2. Equivalent circuit of a solar cell, single diode circuit.

The generated photovoltaic current equation is as follows [34], [35]:

$$I_{PV} = I_{ph} - I_0 \left[exp \frac{\left(V_{pv} + (R_s \times I_s)\right)}{V_t \times \alpha} \right] - \frac{\left(V_{pv} + (R_s \times I_s)\right)}{R_{sh}} \quad (1)$$

where;

$$V_t = \frac{N_S K T}{q} \quad (2)$$

$$I_{ph} = \left(I_{ph,ref} + (K_{I,sc} \times (T - T_{ref}))\right) \frac{G}{G_{ref}} \quad (3)$$

$$I_0 = I_{0,ref} \left(\frac{T_{ref}}{T}\right)^3 \exp\left[\frac{q \times E_g}{\alpha \times k}\left(\frac{1}{T_n} - \frac{1}{T}\right)\right] \quad (4)$$

$$I_{0,ref} = \frac{I_{sc,ref}}{\exp\left(\frac{V_{oc,ref}}{V_{t,ref} \times \alpha}\right) - 1} \quad (5)$$

The parameters of the solar system are given in Table 1.

B. THE MOTOR-PUMP SUBSYSTEM

Variable speed centrifugal pumps are widely used in RO desalination systems due to their simplicity and reliability. They supply the desired pressure behind the RO membrane.

An induction motor is used to drive a high-pressure pump, which supplies seawater or brine water to the reverse osmosis unit. High-efficiency induction motor control can be achieved with the help of field control (FOC) methods. However, knowing the speed of the rotor is essential for using this method. In this control approach, the following relations are satisfied on the d-axis: [36]:

$$\Phi_{rd} = \Phi_r \quad \text{and } \Phi_{rd} = 0 \quad (6)$$

The dynamics of the induction motor by field orientation are determined by the following equations [36]:

$$\frac{di_{sd}}{di} = \frac{1}{\delta L_s}\left(-\left(R_s + \left(\frac{L_m}{L_r}\right)^2 R_r\right) i_{sd} + \delta L_s \omega_s i_{sq} + \frac{L_m R_r}{L_r^2} \emptyset_r + V_{sd}\right) \quad (7)$$

TABLE 1. Photovoltaic solar system parameters.

Parameter	Description
I_{PV}	The final current generated at the output in amperes
I_{Ph}	Current from light radiation in amperes
I_{phref}	Nominal current from light radiation in normal condition in amperes
I_O	Diode current in amperes
I_{Oref}	Nominal saturation current of the diode in amperes
I_{Scref}	Short circuit current in normal condition in amperes
T	Cell temperature in Kelvin
T_{ref}	Nominal cell temperature in Kelvin
G	The amount of radiation in watts per square meter
G_{ref}	Nominal amount of radiation in watts per square meter
q	Electron electric charge in Coulomb (=1.602×10^{-19})
E_g	Gap band energy (=1.381×10^{-23})
K	Boltzmann constant in joules per Kelvin (=1.381×10^{-23})
K_{Isc}	Ratio of short circuit current to thermal coefficient
α	The ideal coefficient of the diode
V_t	Thermal voltage
V_{PV}	The final voltage produced in volts
V_{ocref}	Open circuit voltage in volts
R_s	Equivalent series resistance in ohms
R_{sh}	Equivalent parallel resistance in ohms

$$\frac{di_{sq}}{di} = \frac{1}{\delta L_s}\left(-\delta L_s \omega_s i_{sq} - \left(R_s + \left(\frac{L_m}{L_r}\right)^2 R_r\right) i_{sd} - \frac{L_m}{L_r}\emptyset_{r\omega_r} + V_{sd}\right) \tag{8}$$

$$\frac{d\emptyset_{rd}}{dt} = \frac{L_m R_r}{L_r} i_{sd} - \frac{R_r}{L_r}\emptyset_r \tag{9}$$

$$T_{em} = \frac{PL_m}{L_r} i_{sq}\emptyset_r \tag{10}$$

where i_{sd}, i_{sq} are the stator currents, $\emptyset_{rd}$ is the flux of the rotor, and T_{em} is the electromagnetic torque. The parameter $\sigma = 1 - \frac{L_m^2}{L_s L_r}$ is known as the leakage coefficient. In the pressure controller design process (sub-section 3-2), load (T_L) is considered as the disturbance. Fuzzy-PID controller is used to make the controller robust and also to consider nonlinear effects in the model.

C. REVERSE OSMOSIS MEMBRANE

A membrane which is fed by a pump and two control valves are the elements of the RO subsystem. Neither pre-treatment nor post-treatment unit is considered.

The inlet water is pressurized by a high pressure pump and then fed into the membrane (Fig. 3). This flow is divided into two parts, one part of which enters the bypass part with speed v_b, and the other part enters the membrane (v_{fr}). The current v_{fr} is separated into a stream with low salinity and a stream with high salinity in speed v_r. All output flows are discharged at atmospheric pressure [18], [37].

Reverse osmosis systems are modeled using energy and mass balance equations. The model consists of two ordinary nonlinear differential equations (ODEs) [37], [38], which can describe the process described in Fig. 3 as follows:

$$\begin{cases} \frac{d_{vb}}{dt} = \frac{A_P^2}{A_m K_m V}\left(v_f - v_b - v_b\right) + \frac{A_P}{\rho V}\Delta\pi - \frac{1}{2}\frac{A_P e_{vb} v_b^2}{V} \\ \frac{d_{vr}}{dt} = \frac{A_P^2}{A_m K_m V}\left(v_f - v_b - v_b\right) + \frac{A_P}{\rho V}\Delta\pi - \frac{1}{2}\frac{A_P e_{vr} v_b^2}{V} \end{cases} \tag{11}$$

Bypass flow speed v_b and concentrated fluid speed v_r are the system state variables. V is the total internal volume, A_p is the area of the membrane, K_m is the membrane mass transfer parameter, $\rho$is the density of the fluid, e_{vr} is the concentrated flow valve resistance, e_{vb} is the bypass flow valve resistance, v_f is the feed rate, and $\Delta\pi$ is the osmotic pressure. Low salinity water flow velocitiy v_p and system pressures P_{sys} are defined as follows:

$$v_P = \frac{A_m K_m}{\rho A_P}(P_{sys} - \Delta\pi) \tag{12}$$

$$P_{sys} = \frac{\rho A_P}{A_m K_m}\left(v_f - v_b - v_r\right) + \Delta\pi \tag{13}$$

T the osmotic pressure is computed as follows:

$$\Delta\pi = \delta C_{eff}(T + 273) \tag{14}$$

where:

$$C_{eff} = C_{feed}\left(a + (1-a)\left(\frac{(1-R) + R(v_f - v_b)}{v_f}\right)\right) \tag{15}$$

where C_{feed} shows the TDS (total amount of dissolved solids) of the in the inlet water, δ is related to the effective concentration to osmotic pressure, a is an effective concentration

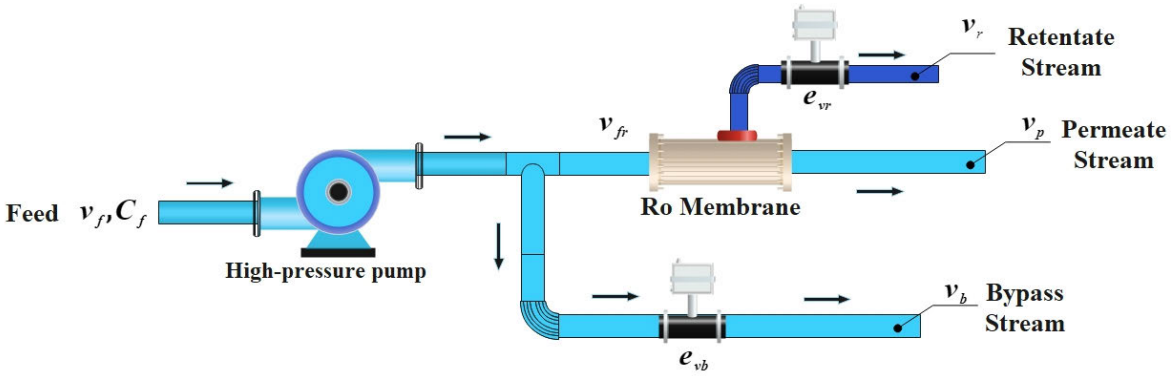

FIGURE 3. Schematic diagram of the desalination process in the reverse osmosis system.

weighting coefficient, R is the minimum salt excretion from the membrane, and T is the temperature of the process.

III. CONTROL STRATEGY

The PV-RO desalination system should be able to withstand different uncertainties in all parts of the system; in the PV system, such as changing the radiation intensity and temperature, in the motor-pump system, such as changing in rotor resistance, and RO system, such as inlet water temperature, inlet water TDS (sea or brackish water). Therefore, a robust control strategy is essential to have a safe and reliable performance.

To achieve maximum power in the solar photovoltaic system in dealing with radiation and temperature changes, a boost converter is used. The duty cycle of the boost converter is controlled by an optimized fuzzy controller. The fuzzy controller is optimized using the invasive weed algorithm (IWA). The induction motor is controlled by the field-oriented control (FOC) strategy. Field-oriented control (FOC) or vector control is a variable-frequency drive (VFD) control strategy that the stator currents of a three-phase AC are identified as two orthogonal components.

The inverter produces a wave with variable frequency output. The mechanical energy is converted to hydraulic energy by the pump-motor subsystem and provides the pressure required for the reverse osmosis membrane.

The control system has three outputs, two of which are related to the output flow rates of the reverse osmosis membrane, and the other is the pressure behind the membrane. The pressure is controlled using a fuzzy-PID controller, and the two discharge outputs are controlled using the state-dependent Riccati equation control.

For each part, a robust control strategy is considered using its dynamic model.

A. OPTIMAL FUZZY CONTROL FOR PV SUBSYSTEM (MPPT CONTROLLER)

A maximum power point (MPP) tracker is an electronic device that permits the PV-system to work at its highest power in different temperature and sun radiation conditions. The maximum power is achieved by adjusting the duty cycle of the boost converter [39], [40], [41].

The goal of MPPT problems is to ensure that the maximum power transfer theorem in electrical circuits is established. This theorem states that to reach the maximum output power from a source with a certain internal resistance, the load resistance must be equal to the internal resistance of the source, which is called impedance matching.

When the load resistance and source resistance as well as load reactance and source reactance are equal, the maximum power is transferred based on maximum power transfer theorem. In a DC circuit, only the resistances must be equal for satisfaction of the theorem conditions. A boost converter can do this. The duty of a boost converter is setting up the input voltage to a higher level required by the load. This is done by adjustment of the duty cycle; sorting energy in an inductor and releasing it to the load.

Because the current and voltage produced by the panel are highly dependent on environmental conditions, the internal resistance of the panel changes due to changes in the voltage and current produced by the panel. Therefore, assuming the load resistance is constant; the manufacturer's side resistance must be adjusted. One method of impedance matching is the use of power converters that equalize the resistance of both the consumer and the producer. This paper uses a boost converter (chopper circuit).

Various controllers have been introduced so far for MPPT, but one of the simplest is the hill-climbing (HC) method. In this method, the basis of the search is the slope of the diagram, i.e., if it (dP/dV) is positive, the system is on the path to the hill, but if it is negative, it means that the movement is in the opposite direction of the peak, and the power value is moving away from its apex, and zeroing the slope means being at the peak of the P-V diagram [33]. Changes in the duty cycle are applied by subtracting or adding a constant number (assuming 0.05 here) to it. Then, the power change is analyzed; if the power is higher than before, the following change will be applied in the same direction. Otherwise, it will be in the opposite direction of the first perturbation. This method is straightforward, but when it reaches the peak

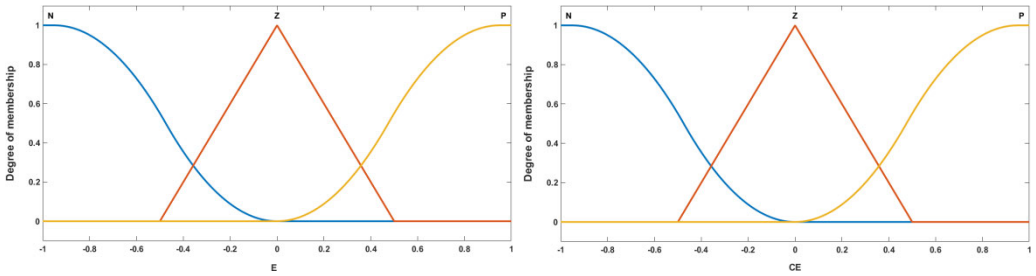

FIGURE 4. Inputs membership functions for the PV system MPPT fuzzy controller.

point, each change, no matter in which direction, leads to a decrease in power, which causes fluctuations in the output and thus increases power losses.

Recently, it is shown that using the feedback control strategies gets better performances in MPPT. A comprehensive review on the application of sliding mode control was done in [42]. Moreover, a review of topologies for I–V curve tracer was presented in [43]. There is a review on the intelligent solar photovoltaic MPPT techniques in [44]. Intelligent control strategies are very popular due to their ease of use and their robustness [45]. Besides, the use of optimized fuzzy controllers with meta-heuristic algorithms has received much attention [46], [47], [48], [49]. These methods have a much better performance compared to classical methods such as the hill-climbing method. In this paper, we use an optimized fuzzy controller with the invasive weed algorithm to reach the maximum power point in different radiation and temperature conditions.

Error (E) and the change of error (CE) are the inputs of the fuzzy controller and defined as follows:

$$E = \frac{P_t - P_{t-1}}{V_t - V_{t-1}} \tag{16}$$

$$CE = E_t - E_{t-1} \tag{17}$$

where P_t is the power and V_t is the voltage at time t. In other words, E shows the slope of the P-V diagram. When error and its change become zero, the system is at its maximum power. For each input, three membership functions are considered as shown in Fig. 4; Negative (N), Zero (Z), and P (positive).

In the proposed fuzzy MPPT controller, as shown in Fig. 4, only three membership functions in the range [-1,1] are considered for simplicity in structure. Then, the two gains, K_1 and K_2, are considered for adjusting the performance of the system (Fig. 6). In other words, the proposed fuzzy MPPT controller not only has a simple and low computational-cost structure but also it can be used for other PV systems by only adjusting the two gains, K_1 and K_2.

The output of the fuzzy controller is the duty cycle of the boost converter. The membership functions of the output are presented in Fig. 5; Small (S), Medium (M), and Big (B).

The structure of the fuzzy controller is shown in Fig. 6. As shown in this figure, two tuning gains K_1 and K_2, are regarded. These two gains and the fuzzy rule-base should

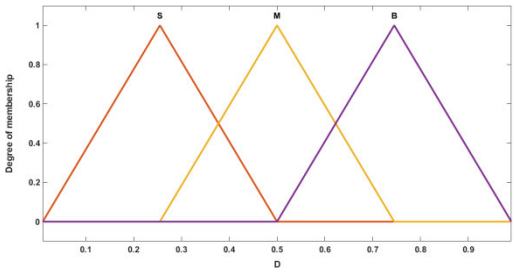

FIGURE 5. Output membership functions for the PV system MPPT fuzzy controller.

be adjusted to optimize the performance of the controller. The invasive weed algorithm (IWA) is used to optimize the performance of the fuzzy controller considering the following performance index:

$$Cost\ Function = \sum \left(\frac{100}{P_{OUT}}\right)^2 \tag{18}$$

The flowchart of the IWA is shown in Fig. 7.

The optimized gain are $K_1 = 0.15$ and $K_2 = 70$. The optimized rule-base is presented in Table 2.

For example, as shown in Table 2, when the error and its change are exactly zero, the following rule is activated:

if E is Z and CE is Z then D is M

If the error and its change be exactly zero, being at the maximum power, the duty cycle will be 0.5, i.e. the center of the membership function M.

When the error is negative, the system is at the left of the pick power in the P-V curve based on Eq. 16. The value of the duty cycle D is dependent on the change of error value (Table 2). If the change of error value is exactly zero, the system is in the vicinity of the maximum power, and the duty cycle is computed based on the following rules:

if E is Z and CE is Z then D is M

if E is N and CE is Z then D is S

B. THE MOTOR-PUMP SUBSYSTEM FUZZY CONTROLLER

The dynamics of the pump and motor are coupled. Moreover, the pump load (T_L) is unknown and is considered as a disturbance. So, a fuzzy-PID controller is designed which

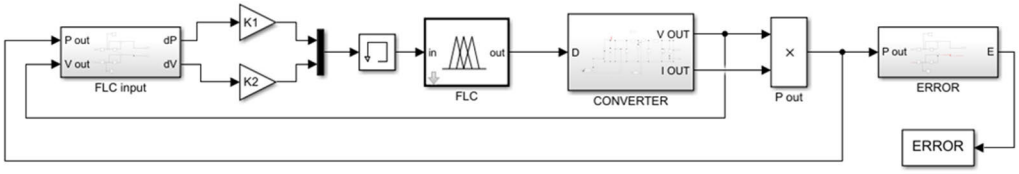

FIGURE 6. MPPT fuzzy controller block diagram.

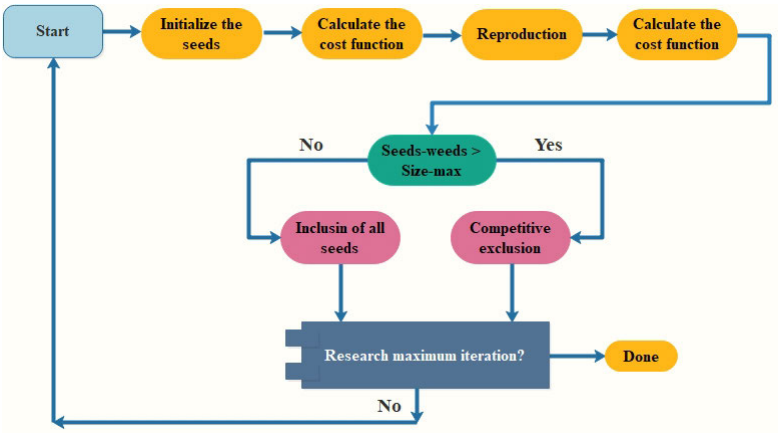

FIGURE 7. IWA flowchart.

TABLE 2. Optimized rule-base for the Fuzzy-IWA controllers.

E / *CE*	N	Z	P
N	M	S	S
Z	S	M	B
P	B	M	M

is robust and suitable for nonlinear systems. In fuzzy-PID controller, the controller gains are derived based on IF-THEN fuzzy rules [50].

In this subsystem, the pressure of the system should be regulated at a desired value which is essential for the RO subsystem performance. The block diagram of this part is shown in Fig. 8. As shown in this figure, two fuzzy controllers are used for speed and pressure regulation. The desired motor speed is derived from pressure loop.

C. RO SUBSYSTEM CONTROLLER

The feed flow rate is considered constant and to control the feed flow into the membrane an actuating bypass valve is considered. The objective of the controller in this subsystem is to stabilize both bypass flow rate and retentate flow rate (flow speeds) as the outputs of the subsystem to their desired values by adjusting the bypass valve and retentate valve (e_{vb}, e_{vr}) as the control inputs (Fig. 3). The proposed controller should not only stabilize the outputs of the subsystem to their desired values but also should be able to compensate for the uncertainties and disturbances.

The SDRE is a sup-optimal controller for nonlinear systems [51], [52], [53], [54]. Its design is systematic and is similar to the LQR theorem for LTI systems.

The SDRE controller is a generalization of the infinite-horizon time-invariant LQR controller for nonlinear systems. The weighting matrices and the algebraic Riccati equation (ARE) are state-dependent. At each time step, these matrices are constant, and the LQ optimal control problem is solved in each time step. Moreover, the LQR controller is robust in dealing with disturbances and uncertainties. In the SISO case, the LQR design has $>60°$ phase margin, infinite gain margin, and a gain reduction tolerance of -6dB. Hence, the SDRE controller is robust similarly.

The nonlinear optimal regulator control method or the State-Dependent Riccati Equation (SDRE) controller solves an algebraic Riccati equation to generate the optimal control law. The unique feature of this method is that due to the state-dependent nature of the coefficients, the Riccati equation is solved in each step with different coefficients. This means that the feedback control gain at each stage is different from the previous stage. The control law is able to actively adjust itself in response to changes in system parameters. In addition, the degrees of freedom of the controller design increase due to the existence of non-unique and state-dependent coefficients.

Consider a nonlinear system as follows:

$$\dot{x} = f(x) + g(x)\,u(t)\,,\, x(0) = x_0 \tag{19}$$

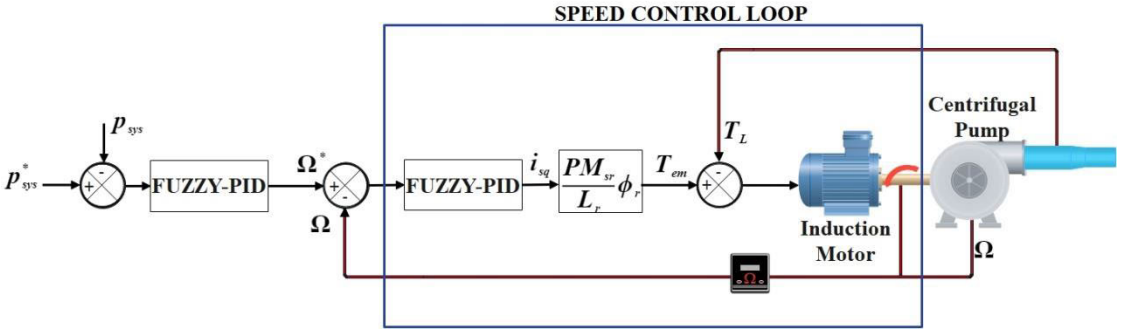

FIGURE 8. Pressure and motor speed control loops.

TABLE 3. Parameters of the system used in simulations.

Parameters of the PV subsystem	
I_{mp}	$7.61\ A$
P_{max}	$200.143\ W$
I_{sc}	$8.21\ A$
V_{oc}	$32.9\ V$
N_s	54
N_p	4
Parameters of the motor-pump subsystem	
P	$750\ W$
R_s	$11.3085\ \Omega$
R_r	$11.8\ \Omega$
L_s	$0.5578\ H$
L_r	$0.6152\ H$
L_m	$0.5578\ H$
J	$0.0020\ kg.m^2$
F	$3.1165 \times 10^{-4}\frac{Nm}{rad\ s}$
p	1
Q_{max}	$30\frac{m^3}{h}$
H	$80\ m$
N	$2900rpm$
Parameters of the RO subsystem	
ρ	$1000\frac{kg}{m^3}$
V	$0.04\ m^3$
A_p	$1.27\ cm^2$
A_m	$30\ m^2$
K_m	$9.218 \times 10^{-9}\frac{s}{m}$
α	0.5
T	$25\ ^\circ C$
R	0.993
δ	0.2641

Suppose $g(x) = B(x)$. Here, $x \in \mathbb{R}^n$, and $u \in \mathbb{R}^m$ are the state and the control inputs vectors, respectively. Also, $f : \mathbb{R}^n \to \mathbb{R}^n$, $B : \mathbb{R}^n \to \mathbb{R}^{n\times m}$, and $B \neq 0, \forall x$. The aim of the controller is to regulate the system outputs to their desired values while optimizing the following performance index:

$$J = \frac{1}{2}\int_0^\infty \left(x^T Q(x)\, x + u^T R(x)\, u\right) dt \qquad (20)$$

where Q(x) is a positive semi-definite weighting matrix and R (x) is a positive-definite weighting matrix. As shown in Eq. (20), a tradeoff between states and control input importance can be considered using Q(x) and R(x) which are state-dependent.

Assumption 1: Function $f(x)$ is continuous differentiable with respect to x for all values of x.

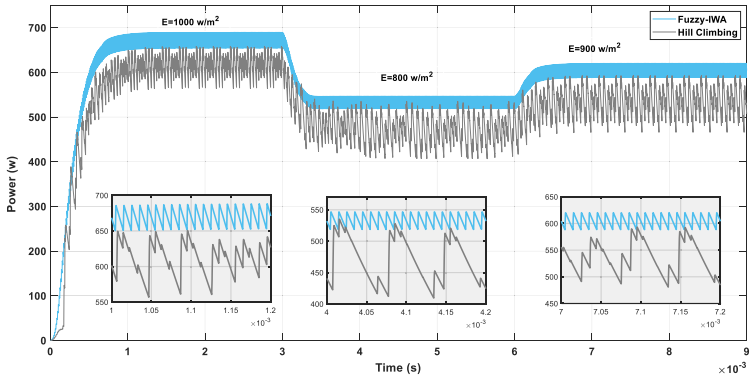

FIGURE 9. Performance of the MPPT fuzzy-IWA controller in comparison with the hill-climbing method.

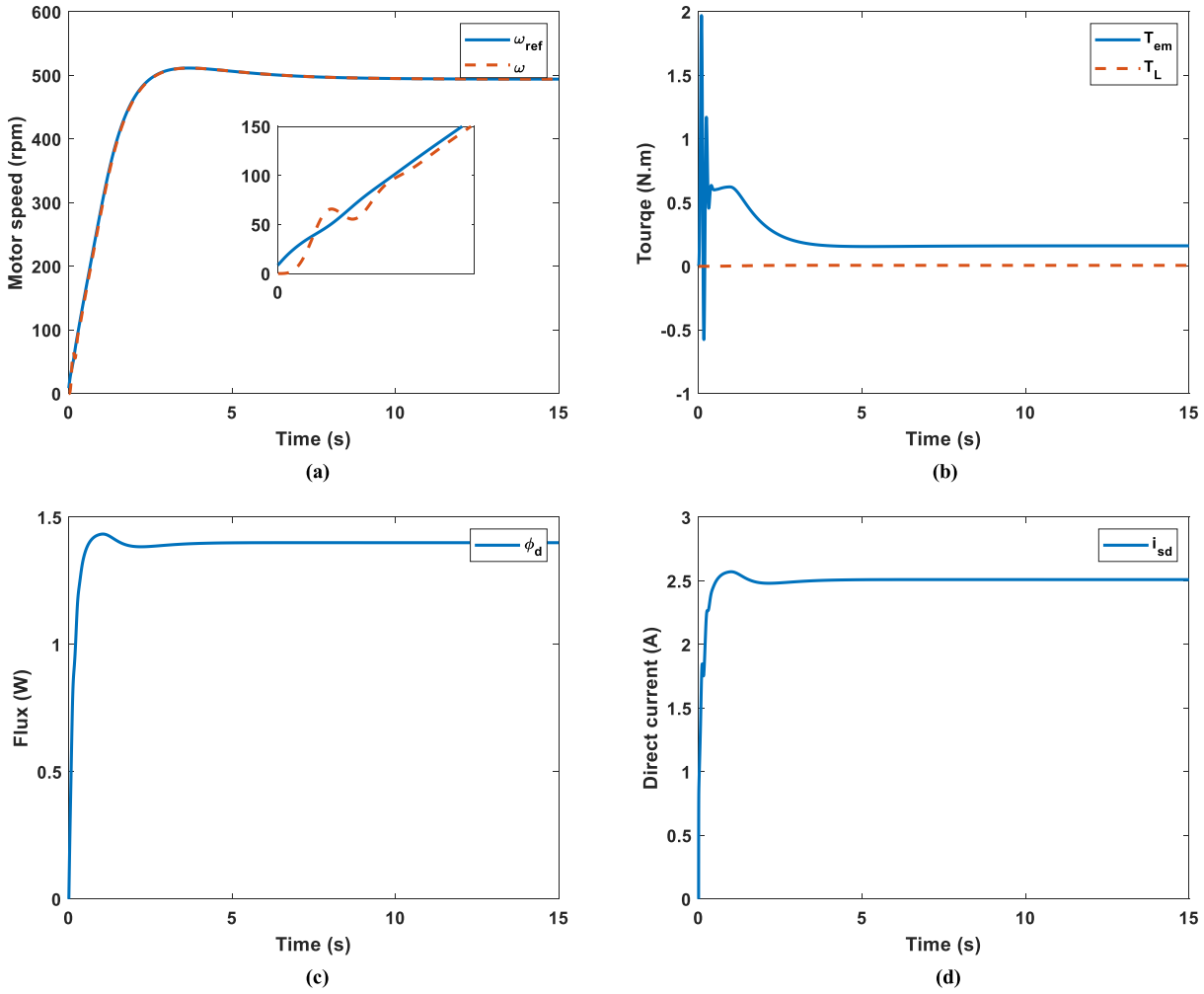

FIGURE 10. Behavior of the motor-pump subsystem; a) Tracking of the desired speed by the induction motor, b) Electromagnetic torque, c) Rotor flux, d) Direct current of the stator.

Assumption 2: The equilibrium point of the system with $u = 0$, is $x = 0$. This means $f(0) = 0$, and $B(0) \neq 0$.

These two assumptions imply the existence of a general state-dependent parameterization for $f(x)$. Therefore, the nonlinear differential equation (19) can be written as (21):

$$\dot{x} = A(x)\,x + B(x)\,u(x), \quad x(0) = x_0,\ f(x) = A(x)\,x \tag{21}$$

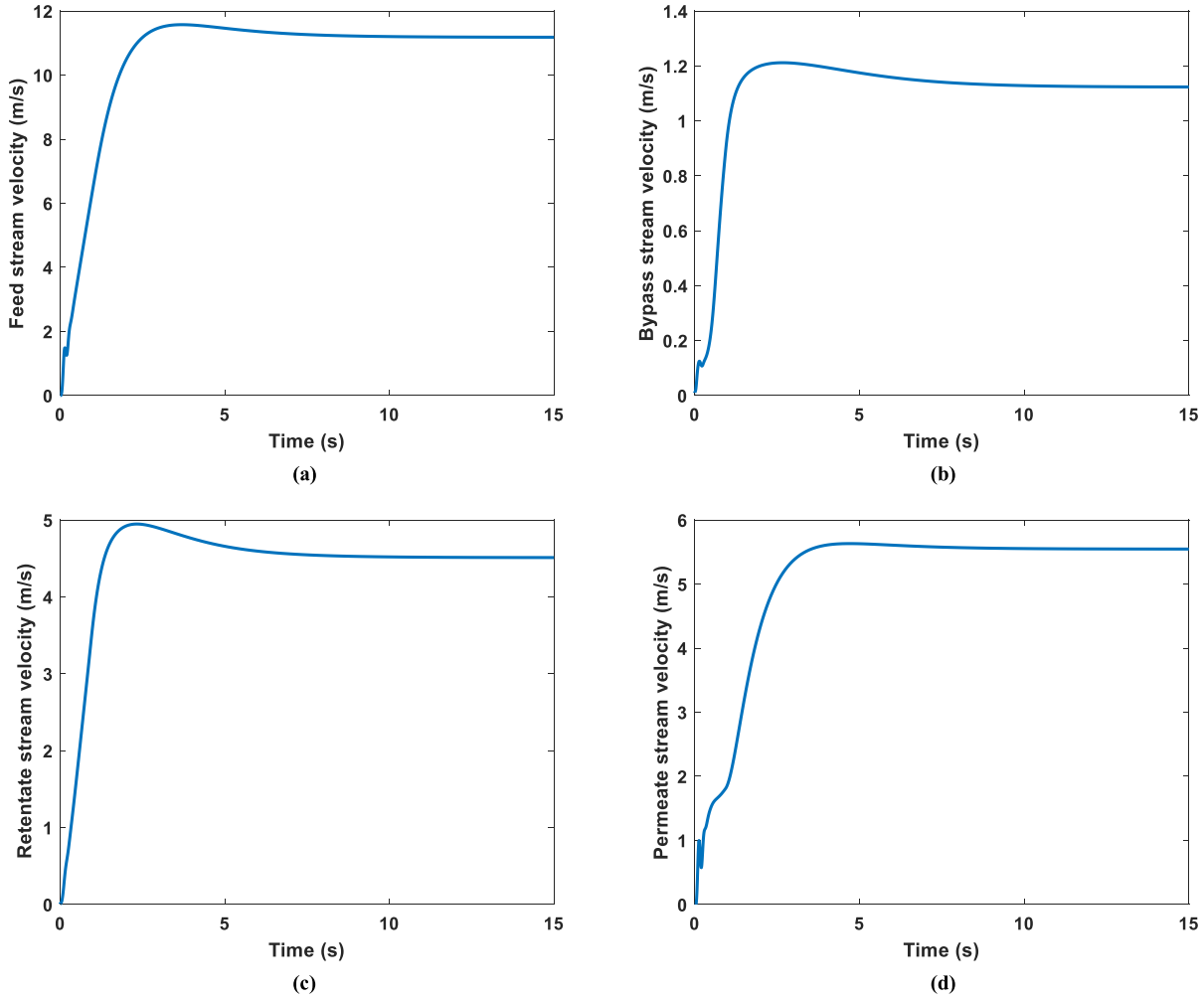

FIGURE 11. Behavior of the Ro subsystem; a) Feed stream speed, b) Speed of the bypass stream, c) Speed of the retentate stream, d) Speed of the permeate stream.

$A(x)$ and $B(x)$ are state-dependent matrices. The following definitions are used for the state-dependent parameterization:

Definition 1: $A(x)$ is a controllable parameterization of the nonlinear system if the pair $\{A(x), B(x)\}$ is controllable for all x.

Definition 2: $A(x)$ is a stabilizable parameterization of the nonlinear system if the pair $\{A(x), B(x)\}$ is stabilizable for all x.

Definition 3: If for all values of x, eigenvalues of $A(x)$ locate in the left hand of imaginary axis, $A(x)$ is Hurwitz.

Also, some more assumptions are made as follows:

Assumption 3: $A(0)$, $B(0)$, $Q(0)$, and $R(0)$ are matrix rated functions $C^1(R^n)$.

Assumption 4: The pairs $A(x), B(x)$ and $\left\{A(x), Q^{\frac{1}{2}}(x)\right\}$ are point stabilized, and observable parameterizations of the nonlinear system (19) for all values of x.

The representation of the matrix $A(x)$ is not unique when the order of the system is 2 and more. When $A_1(x)$ and $A_2(x)$ are two different representation of $f(x)$, another representation cab be as follows:

$$A(x) = \alpha A_1(x) + (1-\alpha) A_2(x), \quad 0 \le \alpha \le 1 \qquad (22)$$

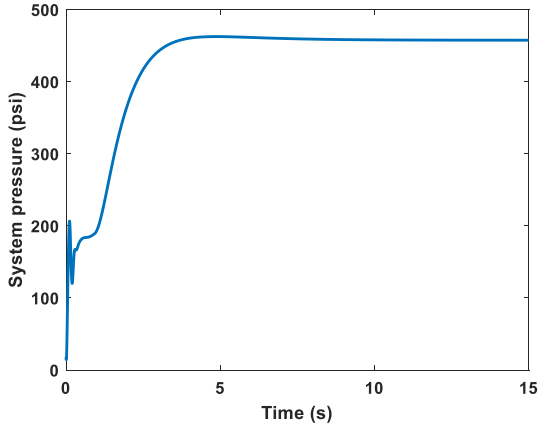

FIGURE 12. Behavior of the system pressure.

The parameter α should be chosen such that the pair $A(x), B(x)$ has more degree of controllability. In other words, the controllability matrix (Φ_c) determinant becomes maximum, where:

$$\Phi_c = \left[B(x)\, A(x)\, B(x) \ldots A^{n-1}(x)\, B(x)\right] \qquad (23)$$

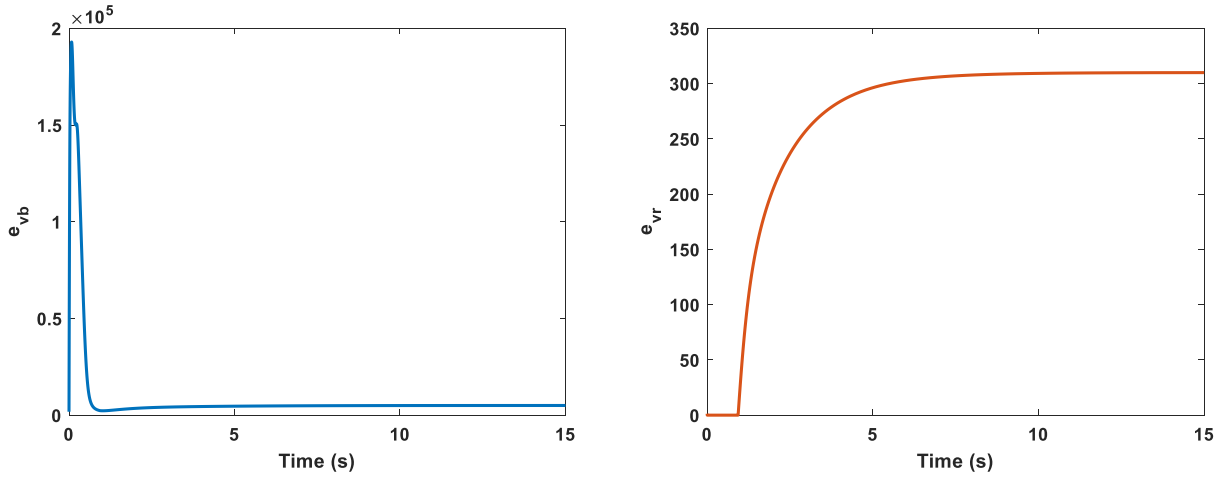

FIGURE 13. Control inputs in the Ro subsystem; e_{vb} and e_{vr}.

The feedback controller will have the same form as the linear mode:

$$u(x) = -R^{-1}(x) B^T(x) P(x) x \tag{24}$$

$P(x)$ is the positive definite solution of the following equation:

$$P(x) A(x) + A^T(x) P(x) - P(x) B(x) R^{-1}(x) B^T(x) P(x) + Q(x) = 0 \tag{25}$$

The closed-loop dynamics is as follows:

$$\dot{x} = \left[A(x) - B(x) R^{-1}(x) B^T(x) P(x)\right] x \tag{26}$$

So, the feedback gain is as follows:

$$K(x) = R^{-1}(x) B^T(x) P(x) \tag{27}$$

As can be seen from these equations, the control gain depends on the x-vector. The advantages of this technique include its simplicity and effectiveness. As observed, no attempt was made to solve the Hamilton-Jacobi-Bellman equation. When the coefficients and weight matrices are constant, the nonlinear optimal regulator problem becomes the well-known linear optimal regulator problem. Asymptotic stability in this method is proved by Lyapunov stability theory.

Stability Proof: Assume that $Q(x)$ is large or $R(x)$ is small enough, so that:

$$\dot{P} - Q - PBR^{-1}B^T P < 0 \tag{28}$$

Therefore, for any state-dependent parameterization, if the nonlinear system is controllable and observable, the closed-loop solution will always be asymptotically stable.

Suppose:

$$V(x) = x^T P(x) x \tag{29}$$

where, $V(x)$ is the Lyapunov candidate function and $P(x)$ is the solution of Riccati equation (25). Due to the observability of $A(x)$:

$$V(x) > 0, \quad P(x) > 0 \tag{30}$$

The derivative of $V(x)$ is:

$$\begin{aligned} \dot{V} &= x^T \dot{P} x + x^T P \dot{x} + \dot{x}^T P x \\ &= x^T \dot{P} x + x^T P \left(Ax - gR^{-1} g^T P x\right) \\ &\quad + \left(Ax - gR^{-1} g^T P x^T\right) P x \\ &= x^T \left(\dot{P} + PA - PBR^{-1} B^T P + A^T P - PBR^{-1} B^T P\right) x \\ &= x^T \left(\dot{P} - Q - PgR^{-1} g^T P\right) x \end{aligned} \tag{31}$$

Therefore, $\dot{V} < 0$ and since parameterization $A(x)$ is controllable and observable, there is a constant $\bar{P} > 0$ such that:

$$V(x) = x^T P(x) x \geq x^T \bar{P} x \tag{32}$$

The above equation determines that when $||x|| \rightarrow \infty$, $V(x) \rightarrow \infty$. So, the equilibrium point in the origin is always asymptotically stable [55]. ■

To track the desired output, the integral controller is used as follows:

$$\dot{e}_b = v_b - v_{b,des} \tag{33}$$

$$\dot{e}_r = v_r - v_{r,des} \tag{34}$$

where $v_{b,des}$ and $v_{r,des}$ are the desired values of v_b and v_r. So, the dynamics of the RO subsystem is as follows:

$$\begin{cases} \dfrac{dv_b}{dt} = \dfrac{A_P^2}{A_m K_m V}\left(v_f - v_b - v_r\right) + \dfrac{A_P}{\rho V}\Delta\pi - \dfrac{1}{2}\dfrac{A_P v_b^2}{V} e_{vb} \\ \dfrac{dv_r}{dt} = \dfrac{A_P^2}{A_m K_m V}\left(v_f - v_b - v_r\right) + \dfrac{A_P}{\rho V}\Delta\pi - \dfrac{1}{2}\dfrac{A_P v_r^2}{V} e_{vr} \\ \dfrac{de_b}{dt} = v_b - v_{b,des} \\ \dfrac{de_r}{dt} = v_r - v_{r,des} \end{cases} \tag{35}$$

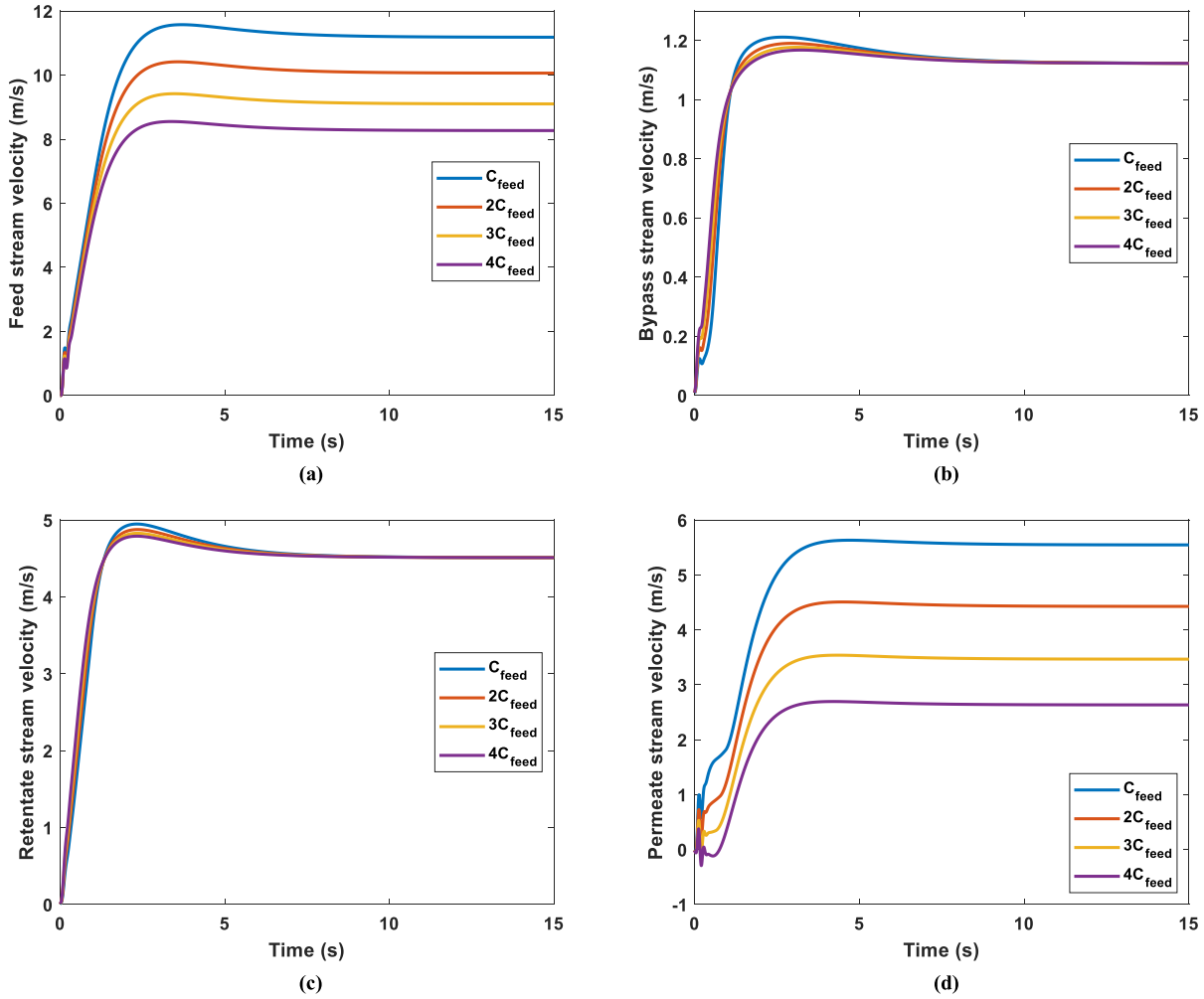

FIGURE 14. Behavior of the Ro subsystem in dealing with changes in the feed water salt concentration; a) Feed stream speed b) Speed of the bypass stream, c) Speed of the retentate stream, d) Speed of the permeate stream.

Matrix A(x), B(x), Q(x), and R(x) are considered as follows:

$$A = \begin{bmatrix} -K_1 & -K_1 & 0 & 0 \\ -K_1 & -K_1 & 0 & 0 \\ 1 & 0 & 0 & 0 \\ 0 & 1 & 0 & 0 \end{bmatrix} \tag{36}$$

$$B = \begin{bmatrix} K_2 v_b^2 & 0 \\ 0 & K_2 v_r^2 \\ 0 & 0 \\ 0 & 0 \end{bmatrix} \tag{37}$$

$$Q = 10^8 v_b \begin{bmatrix} 1 & 0 & 0 & 0 \\ 0 & 1 & 0 & 0 \\ 0 & 0 & 1 & 0 \\ 0 & 0 & 0 & 1 \end{bmatrix} \tag{38}$$

$$R = \begin{bmatrix} 10^{-3} v_b^2 & 0 \\ 0 & 1.5 \times 10^3 v_r \end{bmatrix} \tag{39}$$

where $K_1 = \frac{A_P^2}{A_m K_m V}$ and $K_2 = \frac{1}{2}\frac{A_P v_r^2}{V}$.

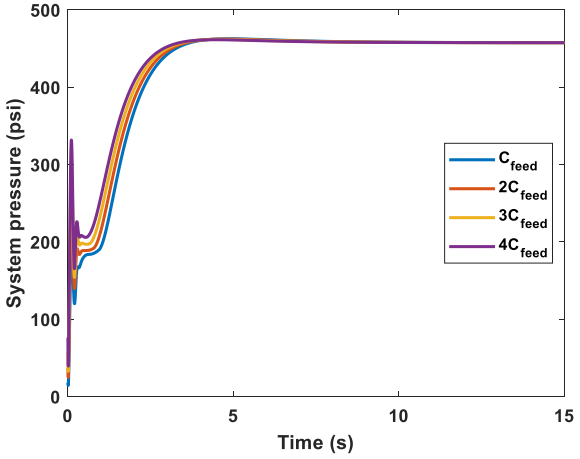

FIGURE 15. System pressure in dealing with changes in the feed water salt concentration.

IV. SIMULATION RESULTS

In this section, several simulations have been done to show the robustness and effectiveness of the proposed controllers.

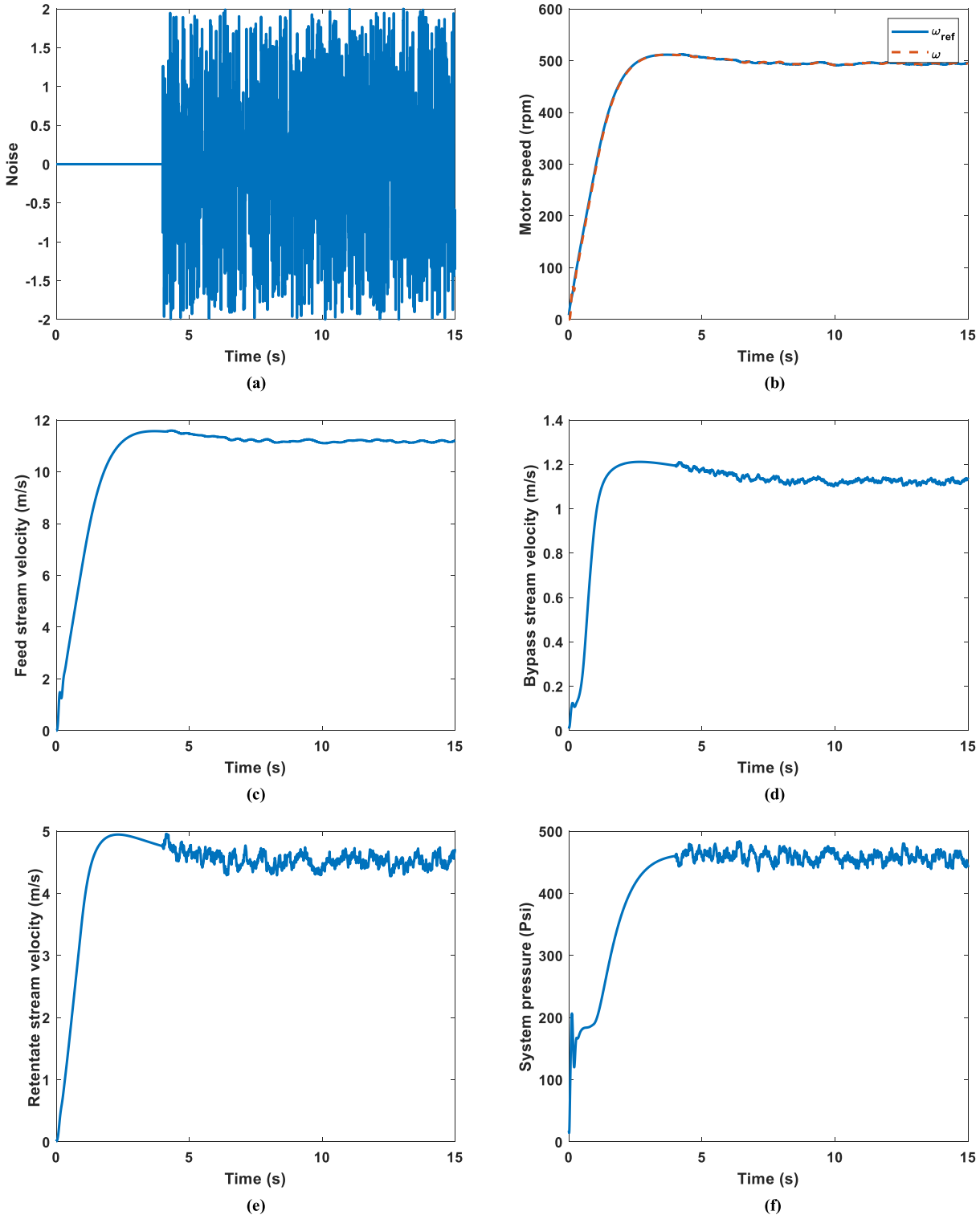

FIGURE 16. Behavior of the system in the presence of noise; a) implemented noise, b) Speed of the motor, c) Speed of the feed stream, d) Speed of the bypass stream, e) Speed of the retentate stream, f) Speed of the permeate stream.

MATLAB/Simulink environment is used for simulation by the parameters of the system are presented in Table 3. The block diagram of the whole system is shown in Fig. 1.

The performance of the IWA-optimized MPPT fuzzy (Fuzzy-IWA) controller in comparison with the hill-climbing method in different radiation intensities is shown in Fig. 9. Solar radiation is started with E = 1000 W/m^2 and changed to

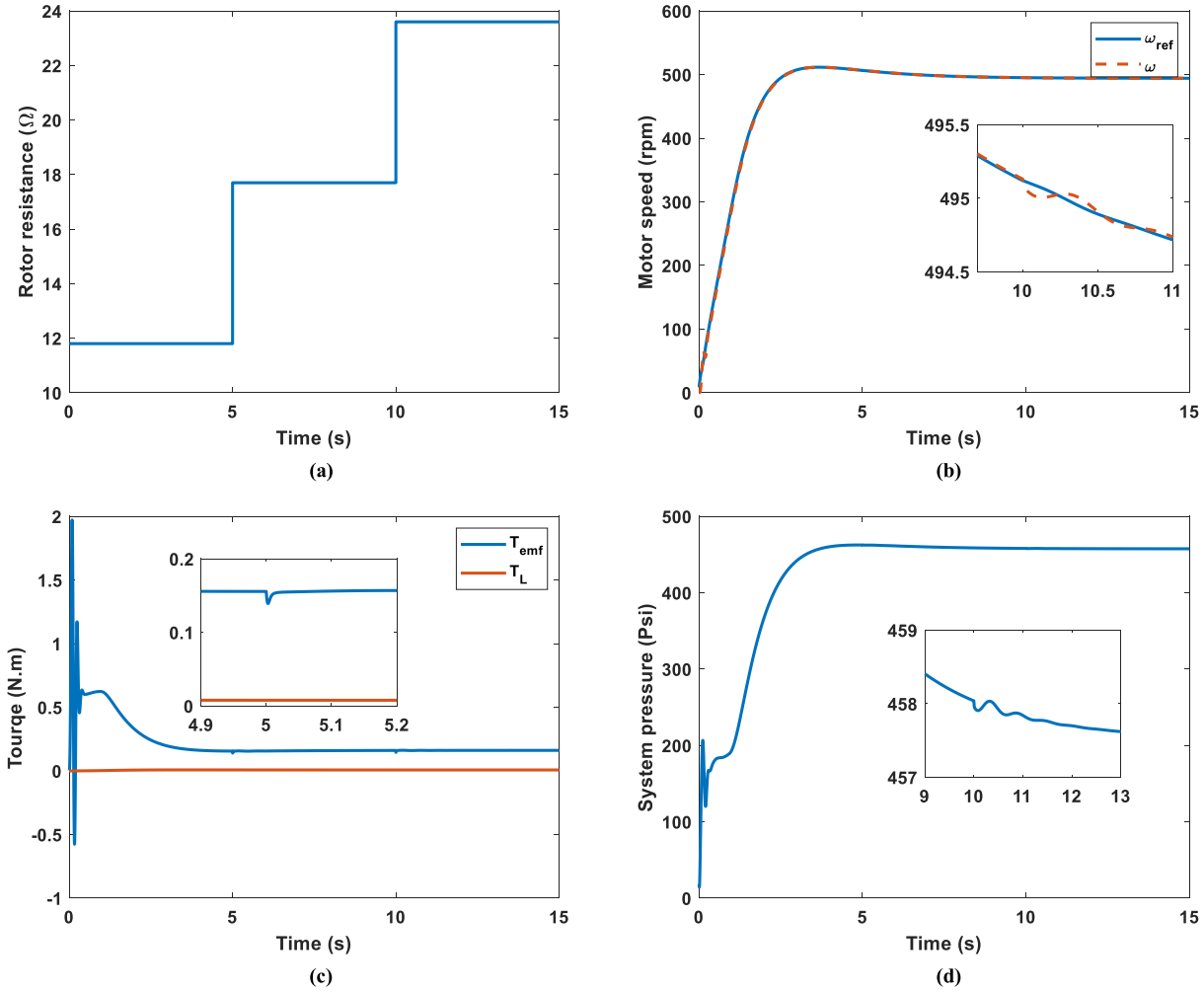

FIGURE 17. Behavior of the system in dealing with changes in rotor resistance; a) Change in rotor resistance, b) Motor speed, c) Torque, d) System pressure.

800 W/m^2 at time t = 3 s and then to 900 W/m^2 at time t = 6 s at a constant temperature T = 25 °C. As shown in this figure, the optimized fuzzy controller with the IWA (Fuzzy-IWA) has better performance in achieving maximum power points in comparison with the hill-climbing method. The proposed fuzzy controller not only has fewer fluctuations but also is more robust than the hill-climbing method.

The proposed fuzzy-IWA controller is not only optimal but also has simpler structure and less membership functions which causes faster response time in comparison with other MPPT fuzzy controllers [44], [56], [57]. The fluctuations of the hill-climbing method can be decreased by lowering the sampling time but it increases the rise time. These two problems (rise time and fluctuations) have been eliminated by the fuzzy-IWA controller.

In designing the MMPT controller, the performance of the system may be better by adding more membership functions or using better optimization algorithms. However, it causes more computational costs. Considering a new control structure may cause better MPP tracking. However, the proposed controller does not need the model of the system; in other words, it is a model-free controller.

The behavior of the motor-pump subsystem is presented in Fig. 10. Tracking of the desired speed is done perfectly by the induction motor and the dynamics of tracking is good. As shown in Fig. 8, the desired speed comes from the pressure control loop. So, the appropriate flow rate is fed by the pump into the membrane to supply desired pressure for the RO membrane. The electromagnetic torque, direct stator current, and rotor flux are shown in Figs. 10b-d. The electromagnetic torque is settled to a higher value than T_L to attenuate the effect of friction. As shown, the direct flux is kept constant which is in accordance with the FOC method.

The desired system pressure is $P_{sys} = 457.51\ psi$ [25] which should be reached by adjusting the feed flow rate; and the feed flow rate depends on the induction motor speed. In this study, the feed flow speed is constant (Fig. 11-a) and the feed flow rate into the RO membrane is adjusted by a bypass valve.

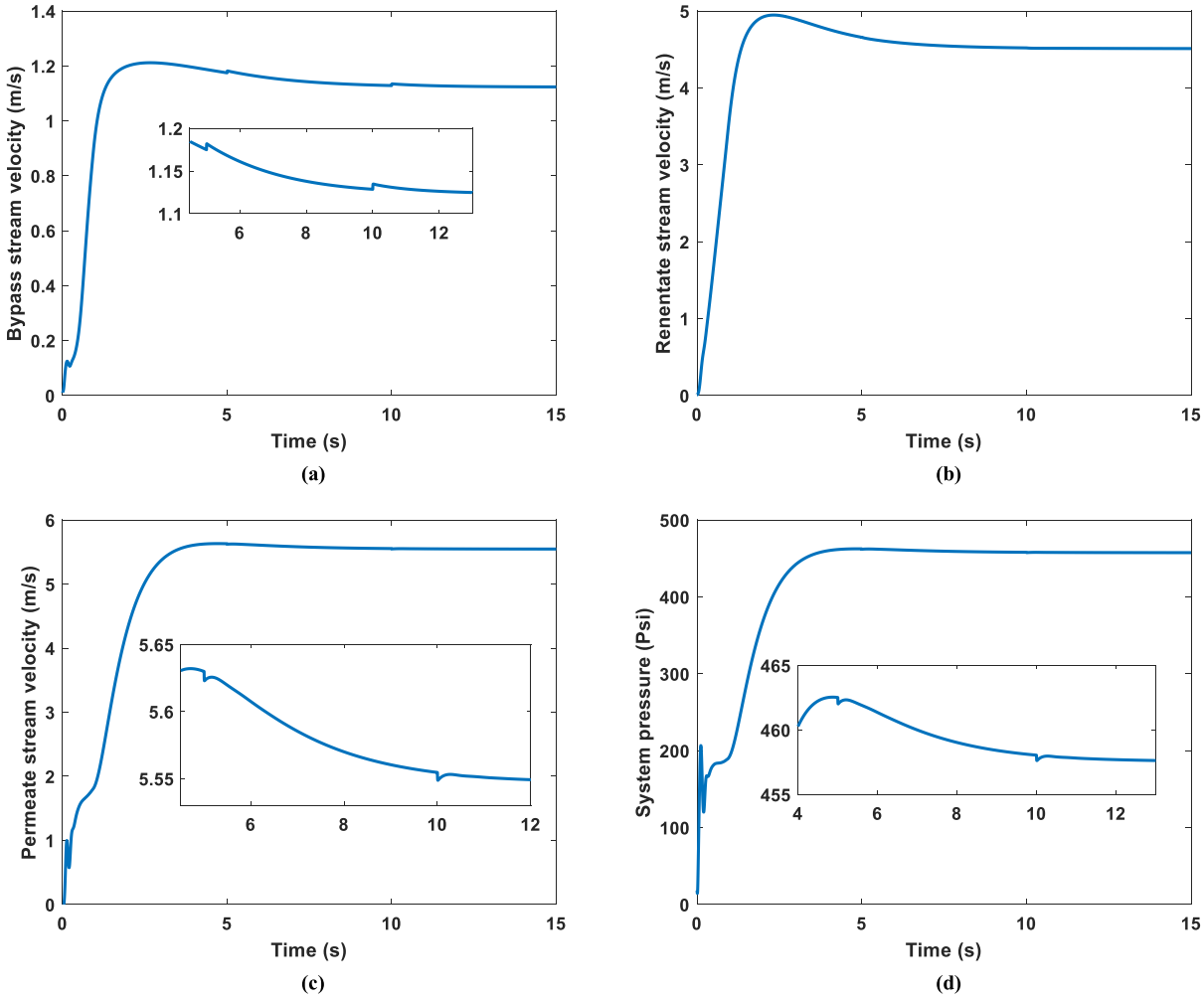

FIGURE 18. Behavior of the system in dealing with faults in bypass valve; a) Speed of the bypass stream, b) Speed of the retentate stream, c) Speed of the permeate stream, d) Pressure of the system.

The desired values of the bypass and retentate flow speeds are set to 1.123 m/s and 4.511 m/s respectively [25]. The behavior of the RO subsystem is shown in Fig. 11 which shows the good performance of the SDRE controller.

Although the SDRE controller is a suboptimal controller with many advantages, especially in practical implementation, it needs the mathematical model of the system. If the mathematical model of the system has many uncertainties, it will affect the performance of the system.

The response of the permeate stream speed is shown in Fig. 11d, which depends on the bypass and retentate stream speeds (Figs. 11b-c). The behavior of the pressure of the system is shown in Fig. 12. As shown in these figures, the rise time and overshoot are appropriate.

The response of the pressure of the system (Fig. 12) shows the good performance of the fuzzy-PID controller. The system pressure is adjusted to its desired values after some deviations which are due to the transient phase of the system. It should be noted that reaching the desired system pressure is essential for the RO subsystem.

The control inputs for the RO subsystem are shown in Fig. 13 which shows that the variation of e_{vb} is more than e_{vr}. At first, e_{vr} is zero and then rises to its final value while e_{vb} increases sharply at first and then settles to its final value.

A. ROBUSTNESS OF THE PROPOSED CONTROLLER

In this section, some variations on the parameters of the system are applied to show the robustness of the proposed controllers. To this aim, changes in feed water concentration, rotor resistance, and noise in outputs are applied.

The performance of the system in dealing with changes in the feed water concentration is shown in Fig. 14. The feed water concentration varies from its nominal value up to four times the nominal value. As shown in this figure, the SDRE controller can overcome the uncertainty in feed water concentration.

As expected, by increasing the feed water concentration, the permeate stream speed decreases (Fig. 14d). This is due to an increase in osmotic pressure which increases the resistance of the flow inside the membrane. So, the feed flow rate must

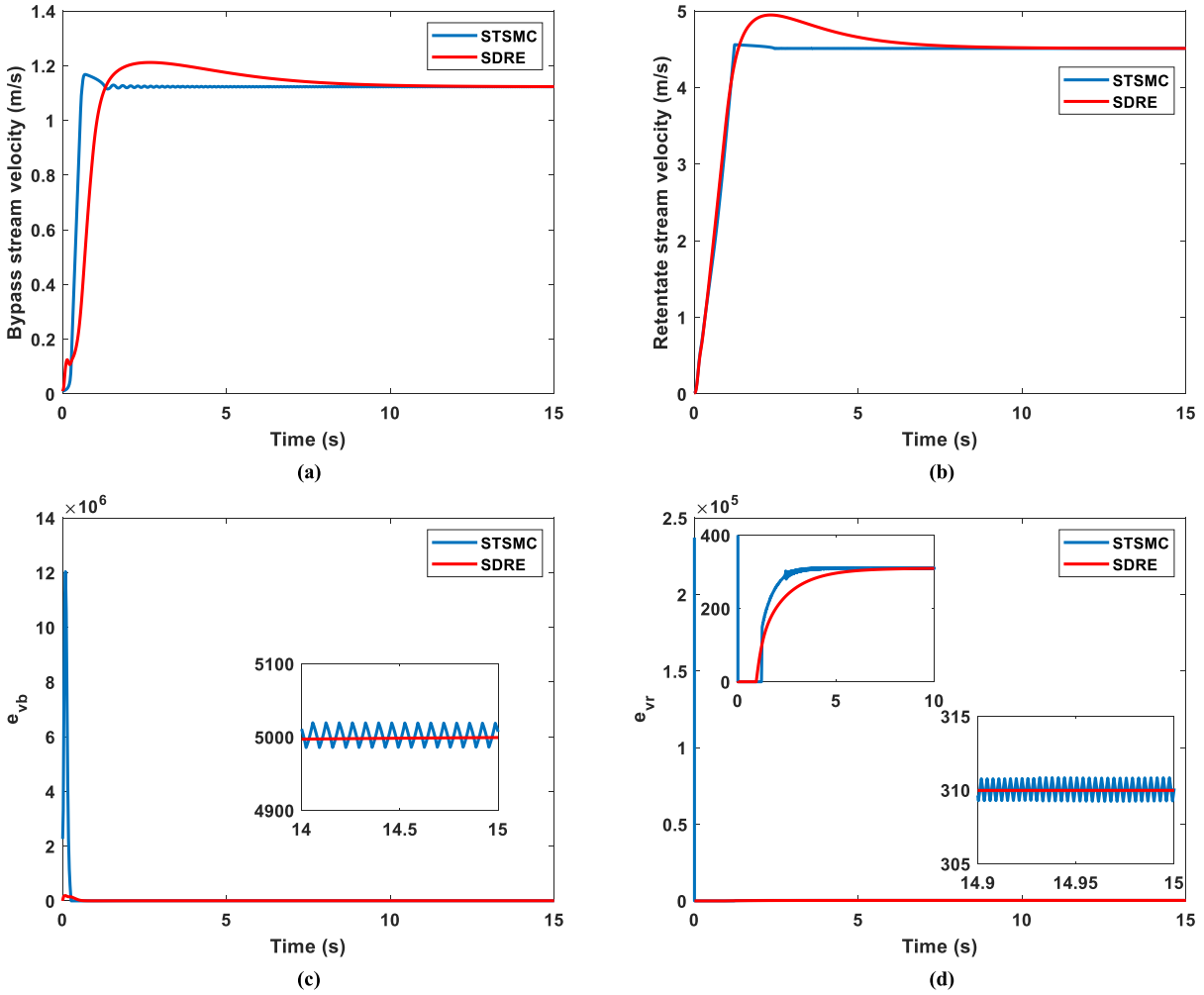

FIGURE 19. Comparison between the super-twisting sliding mode (STSM) control and the state-dependent Riccati equation (SDRE) control; a) Speed of the bypass stream, b) Speed of the retentate stream, c) e_{vb}, d) e_{vr}.

be decreased to preserve the system pressure at its desired value (Fig. 11a). Moreover, the outputs track their desired value with no steady-state error that presents the robustness of the SDRE controller (Figs. 11b-c).

The behavior of the system pressure in dealing with changes in the feed water salt concentration is shown in Fig. 15. As shown in this figure, the fuzzy-PID controller regulates the system pressure to its desired value. Fig. 15 shows that the increase in the feed water salt concentration makes the rise time in the system pressure behavior decreases.

One of the problems in real-world applications is measurement noises. To show the performance of the closed-loop system in the presence of measurement noise, a large white Gaussian noise signal is added to the retentate flow sensor measurement. As shown in Fig. 16, the SDRE controller removes almost 93% of the noise (Fig. 16e) and the outputs of the system track their desired values (Fig. 16b and Figs. 16d-e). As shown in this figure, the bypass stream speed is not affected by noise (Fig. 16d) and the system pressure is near its desired value (Fig. 16f). However, the system pressure is regulated to its desired value. It is proved that the SDRE controller is able to immune the system in dealing with large measurement noises.

B. FAULT TOLERANT CONTROL

The real PV-RO system maybe deals with different faults. So, in this section, the performance of the proposed controller in dealing with faults is considered.

At first, to test the fault-tolerant control of the field-oriented controller (FOC), variations in rotor resistance are considered. Two increases in rotor resistance are imposed, a 50% increase at t=5s and then to 100% at t=10s (Fig. 17a). The behavior of the system in dealing with changes in rotor resistance is shown in Fig.17. As shown in this figure, the closed-loop system has appropriate performance in dealing with changes in rotor resistance.

The tracking of the desired speed is shown in Fig. 17b which shows that the small effect of rotor resistance changes on system behavior. Moreover, the electromagnetic torque remains constant and just a small drop occurs while the rotor

resistance changes. The effect of rotor resistance changes on the system pressure is very small (Fig. 17d).

Fault in the bypass valve is also considered by implementing a 20% and 30% loss in their effectiveness at times t=5s and t=10s, respectively. The behavior of the system in dealing with faults in the bypass valve is shown in Fig. 18. As shown in this figure, the SDRE controller is robust in dealing with faults in the bypass valve. The faults in the bypass valve induce only small deviations in the system response.

In comparison with [25], the SDRE controller has no chattering and its implementation is easier. Moreover, the design flexibility in the SDRE method is higher. The comparison between the super-twisting sliding mode (STSM) control and the state-dependent Riccati equation (SDRE) control is presented in Fig. 19. As shown in this figure, the rise time of the STSMC is smaller than the SDRE method. However, the fluctuations of the system outputs in the STSMC are higher. Moreover, both control inputs e_{vb} and e_{vr} in the STSMC are highly chattering and their changes are more drastic.

V. CONCLUSION

In this paper, the whole subsystems of the PV-RO desalination system consisting of PV generator, induction motor, centrifugal pump, and RO membrane were considered. For each subsystem, i.e. PV subsystem, motor-pump subsystem, and RO subsystem, a controller was designed. For the MPPT of the PV solar system, a new optimized fuzzy controller was designed. The proposed fuzzy controller has a simpler structure and is optimized with the invasive weed (IW) metaheuristic algorithm. For the speed control loop and the pressure control loop, a fuzzy controller was used. Then, a novel application of the SDRE method was used in controlling the RO subsystem. In the RO subsystem, the controller manipulates the bypass and retentate valves. The performance of the whole system was tested numerically in MATLAB/Simulink environment in different uncertain and faulty conditions. Simulation results show the robustness and effectiveness of the proposed controllers.

CONFLICT OF INTEREST

The authors declare that they have no conflict of interest.

DATA AVAILABILITY

Not applicable

REFERENCES

[1] M. A. Abdelkareem, M. El Haj Assad, E. T. Sayed, and B. Soudan, "Recent progress in the use of renewable energy sources to power water desalination plants," *Desalination*, vol. 435, pp. 97–113, Jun. 2018, doi: 10.1016/j.desal.2017.11.018.

[2] E. J. Okampo and N. Nwulu, "Optimisation of renewable energy powered reverse osmosis desalination systems: A state-of-the-art review," *Renew. Sustain. Energy Rev.*, vol. 140, Apr. 2021, Art. no. 110712, doi: 10.1016/j.rser.2021.110712.

[3] United Nations World Water Assessment Programme, *The United Nations World Water Development Report 2015: Water for a Sustainable World*. Paris, France: UNESCO, 2015.

[4] M. Prisciandaro, M. Capocelli, V. Piemonte, and D. Barba, "Process analysis applied to water reuse for a 'closed water cycle' approach," *Chem. Eng. J.*, vol. 304, pp. 602–608, Nov. 2016, doi: 10.1016/j.cej.2016.06.134.

[5] J. R. Ziolkowska and R. Reyes, "Impact of socio-economic growth on desalination in the U.S.," *J. Environ. Manage.*, vol. 167, pp. 15–22, Feb. 2016, doi: 10.1016/j.jenvman.2015.11.013.

[6] A. Matin, T. Laoui, W. Falath, and M. Farooque, "Fouling control in reverse osmosis for water desalination & reuse: Current practices & emerging environment-friendly technologies," *Sci. Total Environ.*, vol. 765, Apr. 2021, Art. no. 142721, doi: 10.1016/j.scitotenv.2020.142721.

[7] Y. J. Lim, K. Goh, M. Kurihara, and R. Wang, "Seawater desalination by reverse osmosis: Current development and future challenges in membrane fabrication—A review," *J. Membrane Sci.*, vol. 629, Jul. 2021, Art. no. 119292, doi: 10.1016/j.memsci.2021.119292.

[8] J. Tian, X. Zhao, S. Gao, X. Wang, and R. Zhang, "Progress in research and application of nanofiltration (NF) technology for brackish water treatment," *Membranes*, vol. 11, no. 9, p. 662, Aug. 2021, doi: 10.3390/membranes11090662.

[9] H. Sharon and K. S. Reddy, "A review of solar energy driven desalination technologies," *Renew. Sustain. Energy Rev.*, vol. 41, pp. 1080–1118, Jan. 2015, doi: 10.1016/j.rser.2014.09.002.

[10] A. M. Bilton, L. C. Kelley, and S. Dubowsky, "Photovoltaic reverse osmosis—Feasibility and a pathway to develop technology," *Desalination Water Treatment*, vol. 31, nos. 1–3, pp. 24–34, Jul. 2011, doi: 10.5004/dwt.2011.2398.

[11] V. N. X. Que, D. Van Tuan, N. N. Huy, and V. Le Phu, "Design and performance of small-scale reverse osmosis desalination for brackish water powered by photovoltaic units: A review," in *IOP Conf. Earth Environ. Sci.*, vol. 652, no. 1, 2021, pp. 1–14, doi: 10.1088/1755-1315/652/1/012024.

[12] M. A. Soleimanzade and M. Sadrzadeh, "Deep learning-based energy management of a hybrid photovoltaic-reverse osmosis-pressure retarded osmosis system," *Appl. Energy*, vol. 293, Jul. 2021, Art. no. 116959, doi: 10.1016/j.apenergy.2021.116959.

[13] M. A. Eltawil, Z. Zhengming, and L. Yuan, "A review of renewable energy technologies integrated with desalination systems," *Renew. Sustain. Energy Rev.*, vol. 13, no. 9, pp. 2245–2262, 2009, doi: 10.1016/j.rser.2009.06.011.

[14] A. Mostafaeipour, M. Qolipour, M. Rezaei, and E. Babaee-Tirkolaee, "Investigation of off-grid photovoltaic systems for a reverse osmosis desalination system: A case study," *Desalination*, vol. 454, pp. 91–103, Mar. 2019, doi: 10.1016/j.desal.2018.03.007.

[15] M. T. Mito, X. Ma, H. Albuflasa, and P. A. Davies, "Reverse osmosis (RO) membrane desalination driven by wind and solar photovoltaic (PV) energy: State of the art and challenges for large-scale implementation," *Renew. Sustain. Energy Rev.*, vol. 112, pp. 669–685, Sep. 2019.

[16] I. Alatiqi, H. Ettouney, and H. El-Dessouky, "Process control in water desalination industry: An overview," *Desalination*, vol. 126, nos. 1–3, pp. 15–32, 1999, doi: 10.1016/S0011-9164(99)00151-4.

[17] I. M. Alatiqi, A. H. Ghabris, and S. Ebrahim, "System identification and control of reverse osmosis desalination," *Desalination*, vol. 75, pp. 119–140, Jan. 1989, doi: 10.1016/0011-9164(89)85009-X.

[18] B. D. H. Phuc, S. S. You, T. W. Lim, and H. S. Kim, "Dynamical analysis and control synthesis of RO desalination process against water hammering," *Desalination*, vol. 402, pp. 133–142, Jan. 2017, doi: 10.1016/j.desal.2016.09.023.

[19] C. W. McFall, A. Bartman, P. D. Christofides, and Y. Cohen, "Control and monitoring of a high recovery reverse osmosis desalination process," *Ind. Eng. Chem. Res.*, vol. 47, no. 17, pp. 6698–6710, Sep. 2008, doi: 10.1021/ie071559b.

[20] A. R. Bartman, P. D. Christofides, and Y. Cohen, "Nonlinear model-based control of an experimental reverse-osmosis water desalination system," *Ind. Eng. Chem. Res.*, vol. 48, no. 13, pp. 6126–6136, Jul. 2009, doi: 10.1021/ie900322x.

[21] S. Chu, S. Zhang, X. Ma, Y. Li, D. Qiu, W. Ge, and L. Kou, "Experimental study on the influence of flexible control on key parameters in reverse osmosis desalination," *IEEE Access*, vol. 10, pp. 4844–4860, 2022, doi: 10.1109/ACCESS.2021.3140071.

[22] K. Alshehri, M. Elshafei, and A. Sheikh, "Maximum power point tracking of directly driven PV-RO systems," in *Proc. 9th Asian Control Conf. (ASCC)*, Jun. 2013, pp. 1–5, doi: 10.1109/ASCC.2013.6606070.

[23] A. B. Chaabene and A. Sellami, "A novel control of a reverse osmosis desalination system powered by photovoltaic generator," in *Proc. Int. Conf. Electr. Eng. Softw. Appl.*, Mar. 2013, pp. 1–6, doi: 10.1109/ICEESA.2013.6578376.

[24] A. Gambier, T. Miksch, and E. Badreddin, "Fault-tolerant control of a small reverse osmosis desalination plant with feed water bypass," in *Proc. Amer. Control Conf.*, Jun. 2010, pp. 3611–3616, doi: 10.1109/acc.2010.5530596.
[25] M. Zebbar, Y. Messlem, A. Gouichiche, and M. Tadjine, "Super-twisting sliding mode control and robust loop shaping design of RO desalination process powered by PV generator," *Desalination*, vol. 458, pp. 122–135, May 2019, doi: 10.1016/j.desal.2019.02.011.
[26] H. Darvishnezhad, M. Nazari, M. Nazari, and M. M. Shahmardan, "Robust control of integrated reverse osmosis desalination system with photovoltaic power supply," *Amirkabir J. Mech. Eng.*, vol. 54, no. 3, p. 5, 2022.
[27] N. Patnana, S. Pattnaik, and V. P. Singh, "Salp swarm optimization based controller design for photovoltaic reverse osmosis plant," *J. Inf. Optim. Sci.*, vol. 41, no. 2, pp. 651–659, Feb. 2020, doi: 10.1080/02522667.2020.1733198.
[28] A. Joseph and V. Damodaran, "Event-driven enabled regression aided multi-loop control for SEC minimisation in SWRO desalination considering salinity variation," *ISA Trans.*, vol. 119, pp. 221–241, Jan. 2022, doi: 10.1016/j.isatra.2021.02.035.
[29] W. Khiari, M. Turki, and J. Belhadj, "Power control strategy for PV/wind reverse osmosis desalination without battery," *Control Eng. Pract.*, vol. 89, pp. 169–179, Aug. 2019, doi: 10.1016/j.conengprac.2019.05.020.
[30] B. Abdelhalim, B. Abdelhak, B. Noureddine, A. Thameur, L. Abdelkader, and L. Zaghba, "Optimization of the fuzzy MPPT controller by GA for the single-phase grid-connected photovoltaic system controlled by sliding mode," in *Proc. AIP Conf.*, vol. 2190, no. 1, Dec. 2019, Art. no. 020003, doi: 10.1063/1.5138489.
[31] A. Pandey, N. Dasgupta, and A. Mukerjee, "High-performance algorithms for drift avoidance and fast tracking in solar MPPT system," *IEEE Trans. Energy Convers.*, vol. 23, no. 2, pp. 681–689, Jun. 2008, doi: 10.1109/TEC.2007.914201.
[32] I. Anil, P. Fuke, and A. K. Yadav, "MATLAB based modeling of conventional and fuzzy logic controller MPPT techniques for solar PV system," in *Innovations in Electrical and Electronic Engineering* (Lecture Notes in Electrical Engineering), vol. 661. Amsterdam, The Netherlands: Elsevier, 2021, pp. 283–293, doi: 10.1007/978-981-15-4692-1_22.
[33] C. B. N. Fapi, P. Wira, M. Kamta, A. Badji, and H. Tchakounte, "Real-time experimental assessment of Hill Climbing MPPT algorithm enhanced by estimating a duty cycle for PV system," *Int. J. Renew. Energy Res.*, vol. 9, no. 3, pp. 1180–1189, 2019.
[34] R. John, S. S. Mohammed, and R. Zachariah, "Variable step size perturb and observe MPPT algorithm for standalone solar photovoltaic system," in *Proc. IEEE Int. Conf. Intell. Techn. Control, Optim. Signal Process. (INCOS)*, Mar. 2017, pp. 1–6, doi: 10.1109/ITCOSP.2017.8303163.
[35] M. G. Villalva, J. R. Gazoli, and E. R. Filho, "Modeling and circuit-based simulation of photovoltaic arrays," in *Proc. Brazilian Power Electron. Conf.*, Sep. 2009, pp. 1244–1254, doi: 10.1109/COBEP.2009.5347680.
[36] G. Abdelmadjid, B. S. Mohamed, T. Mohamed, S. Ahmed, and M. Youcef, "An improved stator winding fault tolerance architecture for vector control of induction motor: Theory and experiment," *Electr. Power Syst. Res.*, vol. 104, pp. 129–137, Nov. 2013, doi: 10.1016/j.epsr.2013.06.023.
[37] A. R. Bartman, C. W. McFall, P. D. Christofides, and Y. Cohen, "Model-predictive control of feed flow reversal in a reverse osmosis desalination process," *J. Process Control*, vol. 19, no. 3, pp. 433–442, Mar. 2009, doi: 10.1016/j.jprocont.2008.06.016.
[38] A. R. Bartman, A. Zhu, P. D. Christofides, and Y. Cohen, "Minimizing energy consumption in reverse osmosis membrane desalination using optimization-based control," *J. Process Control*, vol. 20, no. 10, pp. 1261–1269, Dec. 2010, doi: 10.1016/j.jprocont.2010.09.004.
[39] M. Kavya and S. Jayalalitha, "A novel coarse and fine control algorithm to improve maximum power point tracking (MPPT) efficiency in photovoltaic system," *ISA Trans.*, vol. 121, pp. 180–190, Feb. 2022, doi: 10.1016/j.isatra.2021.03.036.
[40] X. Li, Q. Wang, H. Wen, and W. Xiao, "Comprehensive studies on operational principles for maximum power point tracking in photovoltaic systems," *IEEE Access*, vol. 7, pp. 121407–121420, 2019, doi: 10.1109/ACCESS.2019.2937100.
[41] M. N. Ali, K. Mahmoud, M. Lehtonen, and M. M. F. Darwish, "An efficient fuzzy-logic based variable-step incremental conductance mppt method for grid-connected pv systems," *IEEE Access*, vol. 9, pp. 26420–26430, 2021.
[42] F. F. Ahmad, C. Ghenai, A. K. Hamid, and M. Bettayeb, "Application of sliding mode control for maximum power point tracking of solar photovoltaic systems: A comprehensive review," *Annu. Rev. Control*, vol. 49, pp. 173–196, Jan. 2020, doi: 10.1016/j.arcontrol.2020.04.011.
[43] Y. Zhu and W. Xiao, "A comprehensive review of topologies for photovoltaic I–V curve tracer," *Sol. Energy*, vol. 196, pp. 346–357, Jan. 2020, doi: 10.1016/j.solener.2019.12.020.
[44] M. Mao, L. Cui, Q. Zhang, K. Guo, L. Zhou, and H. Huang, "Classification and summarization of solar photovoltaic MPPT techniques: A review based on traditional and intelligent control strategies," *Energy Rep.*, vol. 6, pp. 1312–1327, Nov. 2020, doi: 10.1016/j.egyr.2020.05.013.
[45] B. Babes, A. Boutaghane, and N. Hamouda, "A novel nature-inspired maximum power point tracking (MPPT) controller based on ACO-ANN algorithm for photovoltaic (PV) system fed arc welding machines," *Neural Comput. Appl.*, vol. 34, no. 1, pp. 299–317, Jan. 2022, doi: 10.1007/s00521-021-06393-w.
[46] Z. Hu, H. Norouzi, M. Jiang, S. Dadfar, and T. Kashiwagi, "Novel hybrid modified krill herd algorithm and fuzzy controller based MPPT to optimally tune the member functions for PV system in the three-phase grid-connected mode," *ISA Trans.*, vol. 2022, pp. 1–16, Feb. 2022, doi: 10.1016/j.isatra.2022.02.009.
[47] H. Tao, M. Ghahremani, F. W. Ahmed, W. Jing, M. S. Nazir, and K. Ohshima, "A novel MPPT controller in PV systems with hybrid whale optimization-PS algorithm based ANFIS under different conditions," *Control Eng. Pract.*, vol. 112, Jul. 2021, Art. no. 104809.
[48] H. Rezk, M. Aly, M. Al-Dhaifallah, and M. Shoyama, "Design and hardware implementation of new adaptive fuzzy logic-based MPPT control method for photovoltaic applications," *IEEE Access*, vol. 7, pp. 106427–106438, 2019.
[49] T. Sutikno, A. C. Subrata, and A. Elkhateb, "Evaluation of fuzzy membership function effects for maximum power point tracking technique of photovoltaic system," *IEEE Access*, vol. 9, pp. 109157–109165, 2021, doi: 10.1109/ACCESS.2021.3102050.
[50] Z. Y. Zhao, M. Tomizuka, and S. Isaka, "'Fuzzy gain scheduling of PID controllers,'" *IEEE Trans. Syst. Man. Cybern.*, vol. 23, no. 5, pp. 1392–1398, Sep. 1993, doi: 10.1109/21.260670.
[51] T. Çimen, "Systematic and effective design of nonlinear feedback controllers via the state-dependent Riccati equation (SDRE) method," *Annu. Rev. Control*, vol. 34, no. 1, pp. 32–51, 2010.
[52] T. Çimen, "State-dependent Riccati equation (SDRE) control: A survey," *IFAC Proc. Volumes*, vol. 41, no. 2, pp. 3761–3775, 2008, doi: 10.3182/20080706-5-kr-1001.00635.
[53] Z. Wang and Y. Li, "State-dependent indirect pseudospectral method for nonlinear optimal control problems," *ISA Trans.*, vol. 108, pp. 220–229, Feb. 2021, doi: 10.1016/j.isatra.2020.08.041.
[54] R. F. da Costa, O. Saotome, E. Rafikova, and R. Machado, "Fast real-time SDRE controllers using neural networks," *ISA Trans.*, vol. 118, pp. 133–143, Dec. 2021, doi: 10.1016/j.isatra.2021.02.019.
[55] J. R. Cloutier, C. N. D'souza, and C. P. Mracek, "Nonlinear regulation and nonlinear H_∞ control via the state-dependent Riccati equation technique: Part1, theory," in *Proc. 1st Int. Conf. Nonlinear Probl. Aviat. Aerosp.*, May 1996, pp. 117–130, 1996.
[56] M. Z. Abdullah, I. Sudiharto, and R. P. Eviningsih, "Photovoltaic system MPPT using fuzzy logic controller," in *Proc. Int. Seminar Appl. Technol. Inf. Commun., IT Challenges Sustainability, Scalability, Secur. Age Digit. Disruption (iSemantic)*, 2020, pp. 378–383, doi: 10.1109/iSemantic50169.2020.9234200.
[57] S. Farajdadian and S. M. H. Hosseini, "Design of an optimal fuzzy controller to obtain maximum power in solar power generation system," *Sol. Energy*, vol. 182, pp. 161–178, Apr. 2019, doi: 10.1016/j.solener.2019.02.051.

HOSSEIN DARVISHI NEJAD received the B.Sc. degree in mechanical engineering from Islamic Azad University—Sari Branch, in 2018, and the M.Sc. degree in energy conversion from the Shahrood University of Technology, in 2022. His main research interests include renewable energy technologies, desalination, and non-linear controllers.

MOSTAFA NAZARI received the B.Sc., M.Sc., and Ph.D. degrees in mechanical engineering from the K. N. Toosi University of Technology, Tehran, Iran, in 2007, 2009, and 2014, respectively. He has been an Assistant Professor with the Mechanical Engineering Department, Shahrood University of Technology (SUT), Shahrood, since 2015. He teaches courses in the areas of control, robotics, and dynamic system. He has published about 30 articles in peer-reviewed journals and conference proceedings. His research interests include modeling and control of dynamical systems, nonlinear control, and fuzzy control.

MOHSEN NAZARI received the B.Sc. degree from the Shahrood University of Technology (SUT), in 2003, the M.Sc. degree from Sharif University, in 2005, and the Ph.D. degree from Tehran University, in 2010. He completed the Research-Study with the University of Amsterdam, in 2011. He is currently an Associate Professor with the Department of Mechanical and Mechatronics Engineering, SUT. He has authored/coauthored more than 70 reputable journal and conference papers. His research group studies transport phenomena in porous media, drug delivery, electro kinetics, multiphase flow, and desalination. He is a member of the Iranian Association of Elites.

MOHAMMAD MOHSEN SHAH MARDAN received the B.Sc. degree from the Ferdowsi University of Mashhad, in 1989, the M.Sc. degree from the Shahid Bahonar University of Kerman, in 1994, and the Ph.D. degree from Lomonosov Moscow State University, in 2004. He is currently a Professor of mechanical engineering with the Shahrood University of Technology (SUT). His expertise is CFD, heat transfer, and non-newtonian fluids. He has authored/coauthored more than 60 reputable journal and conference papers. He is a member of the Iranian Association of Elites.

ARDASHIR MOHAMMADZADEH (Student Member, IEEE) was born in West Azerbaijan, Iran. He received the B.Sc. degree from the Sahand University of Technology, Tabriz, Iran, in July 2011, the M.Sc. degree from the KT University of Technology, Tehran, Iran, in September 2013, and the Ph.D. degree from the University of Tabriz, Tabriz, in November 2016. In December 2017, he joined as an Assistant Professor with the University of Bonab, Bonab, Iran. In 2022, he joined as an Associate Professor with the Shenyang University of Technology. He has published many articles in most reputed journals. His research interests include control theory, fuzzy logic systems, machine learning, neural networks, intelligent control, electrical vehicles, power systems control, chaotic systems, and medical systems. He is an Academic Editor of *PLOS One* and a Reviewer of several journals, such as IEEE TRANSACTIONS ON FUZZY SYSTEMS, *Applied Soft Computing*, and *Nonlinear Dynamics*.

MAI THE VU received the B.S. degree in naval architecture and marine engineering from the Ho Chi Minh City University of Technology, Vietnam, in 2013, and the Ph.D. degree from the Department of Convergence Study on the Ocean Science and Technology, Korea Maritime and Ocean University, South Korea, in 2019. He is currently an Assistant Professor with the Department of Unmanned Vehicle Engineering, Sejong University, South Korea. His research interests include underwater vehicles and robotics, multi-body dynamic modeling, linear and nonlinear control, trajectory tracking, path planning, obstacle avoidance, and intelligent navigation.

AMIR MOSAVI (Student Member, IEEE) received the bachelor's degree from London Kingston University, U.K., and the Ph.D. degree in applied informatics. He is currently an Associate Professor of computer science interested in big data, the IoT, and machine learning. He is also a Senior Research Fellow at Oxford Brookes University and TU-Dresden. He is a Data Scientist for climate change, sustainability, and hazard prediction. He was a recipient of the Marie Curie Award, the Green-Talent Award, the UNESCO Young Scientist Award, the ERCIM Alain Bensoussan Fellowship Award, the Campus France Fellowship Award, the Campus Hungary Fellowship Award, and the Endeavour-Australia Leadership.